J. Fluid Mech. (1988), *vol.* 195, *pp.* 557–580
Printed in Great Britain

Another approach in modelling cavitating flows

By H. LEMONNIER† AND A. ROWE‡

†Centre d'Etudes Nucléaires de Grenoble, SETh/LEF, 85X, 38041 Grenoble CEDEX, France

‡Centre de Recherches et d'Essais de Machines Hydrauliques de Grenoble, ENSHMG, BP 95, 38402 St Martin d'Heres CEDEX, France

(Received 25 July 1985 and in revised form 5 April 1988)

A cavitating-flow calculation method is presented, based on the panel technique with minimization of a certain vector characterizing the discretion error which may become important under cavitating conditions. Several practical examples are presented: partial cavitation on an isolated foil, cavitation behind a blunt-ended body, and the problem of two cavities around an axisymmetrical body. In the case of partial cavitation, the Joukowski condition and tangential outlet condition can be satisfied by the form of the error vector. The cavity-wake modelling problem is not extensively dealt with. It is shown, however, that in order to obtain a satisfactory cavity length/cavitation number ratio, it is probably necessary to introduce a displacement thickness behind the near wake of the cavity which does not close on the body according to a separated flow scheme analagous to the wake, as introduced previously by Yagamuchi & Kato (1983). The method is shown to be capable, after a few minor modifications, of dealing with the case of bodies with a rounded rear edge. Even so, the advantage is essentially didactic as the problem of predicting the position of separation points is not treated. The problem of two cavities around axisymmetrical bodies has a more obvious practical interest. The nonlinear closure condition of each cavity is exactly satisfied by an iterative resolution scheme in which allowance is made for the presence of an axial gravity field.

1. Introduction

The tasks of designing hydraulic machines and predicting their performance have preoccupied engineers for many years, indeed since before the beginning of the nineteenth century. Today, thanks to the modern computer, it is possible to consider increasingly complex flow conditions without excessive schematization. This is the case, for example, in the design of marine propellers; previously based on Prandtl's lifting-line theory, the design now considers the surface-lifting method which is more suited to geometries of low aspect ratio.

One of the most severe technical requirements imposed on a hydraulic machine is due to cavitation. As it develops, cavitation creates noise, vibration, metal erosion and, finally, a drop in machine performance. Much work has been done in past years to obtain a better understanding of the physical phenomenon of cavitation in order to predict and alleviate its effects on machine performance. Curiously enough, whereas calculations of flow in turbomachines or around propellers have for several years been based increasingly on numerical methods, modelling of cavitating flows has continued to develop, until quite recently, mainly through analytical methods. Could this be the price paid for the popularity of the techniques developed and proven by Wu (1956, 1959), Tulin (1953, 1964), Larock & Street (1967), Leehey (1973), etc., at a time when supercavitation held rich application possibilities.

The analytical calculation of cavitating flows is based on two techniques: the small-perturbation theory proposed by Tulin, and the nonlinear theory that originated from work by Helmoltz, Kirchhoff and Levi-Civita. The analytical calculation of cavitating flows using conformal transformation comes up against two major difficulties: implementation of the nonlinear theory is difficult, and extension to three-dimensional flow is impossible outside the framework of perturbation methods. The most comprehensive analytical developments are probably those proposed by Furaya, whose nonlinear theory dealt successively with the case of a supercavitating section near a free surface (1975*a*), a supercavitating foil near a free surface (1975*b*) and a partially or fully cavitating cascade (1980). In spite of the precautions taken, convergence of the solution is not always certain when the lower side of the foil is arbitrarily shaped. Moreover, the instabilities affecting the position of the cavity detachment point near the leading edge make problematical any procedure aimed at predicting this position by matching with a boundary-layer calculation.

Although there are only a small number of numerical cavitating-flow calculation methods, some of these methods date back to the 1960s. For example, Widnall (1966) treated the case of a supercavitating foil in unsteady flow using the surface-lifting method. In this pioneering work, the cavity closure zone is not defined. In 1969, Nishiyama & Miyamoto treated the problem of a supercavitating foil placed under a free surface. Tsen & Guilbaud (1974) studied the effect of the plan shape of a super-ventilated foil from both experimental and theoretical standpoints. In 1979, Verron extended Tsen & Guilbaud's method to the case of base-vented foils. In this work, the plan shape of the cavity is calculated for non-zero cavitation numbers. The important case of partial cavitation was tackled at MIT by Golden, Uhlman, Jiang and Van Houten between 1975 and 1978. Application to the problem of propellers was accomplished by Chang-Sup in 1980.

In previous studies, boundary conditions have been linearized to varying degrees. In the nonlinear theory, Pellone & Rowe (1981) treated the case of a base-vented foil near a free surface. The method developed by these authors can also be used to treat the case of supercavitating conditions, but the extrapolation to partially cavitating flows is not obvious. The numerical calculation of such flows in nonlinear theory is poorly represented. This problem is not as simple as it appears, especially when the submerged structure has a very small relative thickness. In 1975, Furness & Hutton, treated the case of a cavity in a two-dimensional convergent-divergent nozzle under unsteady flow conditions, according to a method that would be well suited to the calculation of thin structures. The method does not seem to have been applied to industrial situations (to the authors' knowledge). In 1977, Nishiyama & Ito and more recently Yamaguchi & Kato (1983) presented methods well suited to the case of foils having a large relative thickness. These methods have the drawback of not allowing adjustment of the 'overpressure zone' that exists at the rear of the cavity, and they degenerate into extremely simplified schemes when the conditions become non-cavitating.

The model presented here aims to be flexible, simple and adjustable: flexible to allow it to be used under a variety of conditions, simple so that extrapolations to unsteady or three-dimensional flows can be made, and adjustable so that it can be made to fit experimental results. Increasingly complex situations will be illustrated by the following examples: partial cavitation on a thin foil, cavitation behind a rounded body, consideration of the gravity effect in the case of an axisymmetrical body, and simultaneous calculation of two cavities.

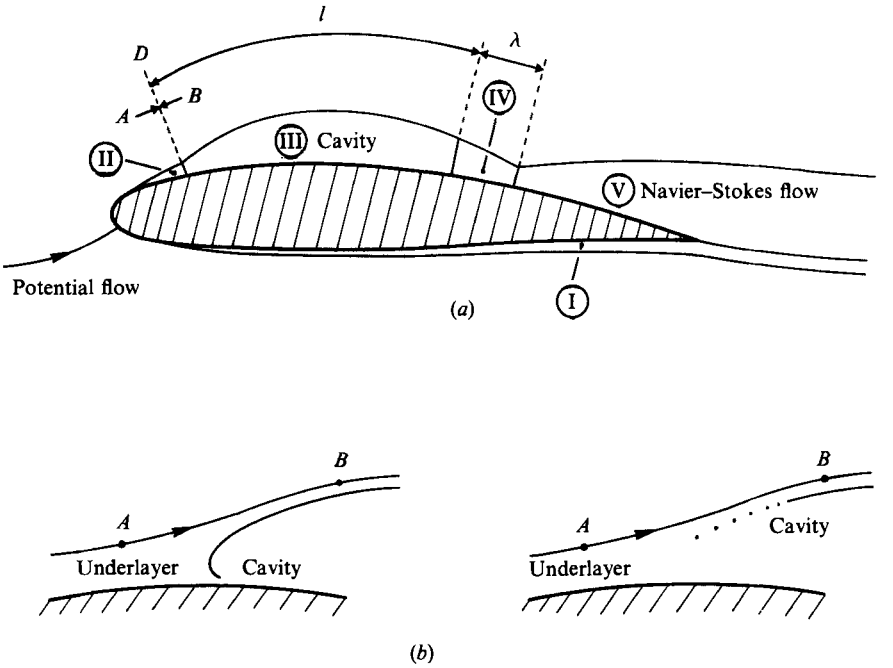

FIGURE 1. (*a*) Flow configuration. (*b*) View of tip cavity.

2. Principle of the method

2.1. *Flow modelling*

The flow field around the foil represented schematically in figure 1 (*a*) includes several domains:

– domains I and II, for which the approximation of the boundary layer remains valid, except at the common boundary between domains II and III;

– domain III, bounded by a constant-pressure streamline;

– domain IV, corresponding to the near wake which is essentially rotational, two-phase and turbulent;

– domain V, called the ultimate wake, corresponding to the diffusion of domain IV in the potential flow.

For simplicity consideration will be given to average steady flow conditions.

Domains I and II can be modelled by displacement thicknesses bounded by a fictitious streamline connecting to the cavity boundary. It will be assumed herein that these domains have zero displacement thickness. By means of a boundary-layer calculation, it should be possible to correct the potential solution to take into account domains I and II, and at the same time to calculate the position of their common boundary with domain III by referring, for example, to the 'laminar separation' criterion. In the vicinity of points *A*, *B* (figure 1*b*) is not absolutely necessary to assume that the tangential outlet condition is satisfied. In other respects, this condition is not always justified from the physical standpoint.

Modelling of domains IV and V creates more serious difficulties. At the present time, there are not sufficiently accurate experimental data available to form the basis of a comprehensive study of the phenomena involved in these regions. Such results are probably not available because the numerical tools currently developed are still

not effective in dealing with the information collected. Therefore this study will be limited to the potential problem and, in the context of a steady flow solution, domain IV is replaced by a displacement thickness connecting to the cavity boundary, and domain V is assumed to be in evanescence. The latter assumption is certainly very restrictive, as domain IV introduces a high level of turbulence and the coupling between domains IV and V is felt throughout the flow.

In what follows, domain IV is characterized by its length, λ, chosen arbitrarily as input data, and by a recompression law given indirectly.

2.2. *Resolution by the method of singularities*

From the various assumptions described in §2.1 above, the problem can be reduced to an integral formulation. In two dimensions, the velocity field is induced by a dual source and vorticity distribution according to equation (1):

$$\boldsymbol{V}(P) = \int_{(s)} \frac{\sigma(M)\,\boldsymbol{r}(M,P)}{r^2(M,P)}\,\mathrm{d}s(M) + \int_{(s)} \frac{\omega(M)\,\boldsymbol{k}\times\boldsymbol{r}(M,P)}{r^2(M,P)}\,\mathrm{d}s(M) + \boldsymbol{V}_\infty, \tag{1}$$

where P is the velocity calculation point, M any point on the domain boundary, $\boldsymbol{r}$ the vector joining M and P, $\mathrm{d}s$ the contour element, σ and ω the source and vorticity distributions, $\boldsymbol{V}_\infty$ the velocity of the undisturbed flow, and $\boldsymbol{k}$ a unit vector normal to the flow plane.

In this equation, the integrals are considered according to Cauchy's principal value when P tends towards S. In the analytical formulation, and depending on the nature of the boundary conditions, it is possible to choose arbitrarily either of the singularity distributions and to calculate the other distribution from these boundary conditions. A single-valued solution is guaranteed, despite the initial indeterminate nature of the singularity distributions.

The discretization of (1), which leads to the classic 'panel method' technique described below, unfortunately destroys this property. For example, in this technique, the choice of a constant-intensity vorticity distribution gives rise to a systematic error in the lift calculation under subcavitating conditions. In the case of a cavitating-flow calculation, this problem is compounded by another: the existence of different boundary conditions on the two sides of the foil. If the vorticity distribution on the wetted side and the source distribution on the cavity are chosen arbitrarily as input data, an acute problem of connection in the transition zone between the different domains is raised.

For these two reasons, it is necessary to calculate all the singularity distributions according to an objective criterion, rather than choosing part of the distribution arbitrarily. According to ideas put forward by Hunt & Semple (1980) the calculation can be organized around the search for the minimal error associated with a given discretization. It is then essential to describe the body by panels reflecting the geometry as accurately as possible. In what follows, it will be assumed that this problem is solved.

The influence of singularities in the vicinity of the observation point can be summarized by the following equations, up to second order:

$$\boldsymbol{V}_\sigma(P) = -4\Delta s\,\sigma'(P)\,\boldsymbol{t} + \left(2\pi + \frac{2\Delta s}{R(P)}\right)\sigma(P)\,\boldsymbol{n}, \tag{2}$$

$$\boldsymbol{V}_\omega(P) = \left(2\pi + \frac{2\Delta s}{R(P)}\right)\omega(P)\boldsymbol{t} + 4\Delta s\omega'(P)\boldsymbol{n}, \tag{3}$$

where $\boldsymbol{V}_\sigma$ and $\boldsymbol{V}_\omega$ are the source and vorticity components of the disturbance speed, $2\Delta s$ is the length taken into account in the vicinity of point P, $R(P)$ the radius of curvature in P, $\boldsymbol{n}$ the normal unit vector and $\boldsymbol{t}$ the tangential unit vector oriented by the curvilinear abscissa, and where the prime expresses the derivative with respect to the curvilinear abscissa. The subscripts σ and ω relate to sources and vortices respectively.

Equations (2) and (3) show that there are two velocity-generation modes. One is proportional to the intensity of singularities, while the other is proportional to their gradient. The most economical way of discretizing (1) involves discretizing the geometry by straight-line segments and considering the distributions to be constant on these domains. This procedure, which neglects local effects due to the gradients, is acceptable if the couple (σ, ω) is chosen in such a manner that the following conditions are obtained:

$$\Delta s\, \sigma'(P) \quad \text{and} \quad \Delta s\, \omega'(P) \quad \text{minimum}. \tag{4}$$

Such a formulation does not promote either of the two singularity distributions and thus does not introduce any priority for the type of boundary conditions necessary for resolution of the problem.

The numerical evaluation of (4) and their minimization in a weighted least-squares sense involves finding a minimum of a quadratic function of the values of the singularities. The overall problem can be written as follows:

$$\text{boundary conditions} \qquad \boldsymbol{H}\boldsymbol{x} = \boldsymbol{l}, \tag{5a}$$

$$\text{minimization criterion} \quad \boldsymbol{e} = \boldsymbol{E}\boldsymbol{x}; \quad |\boldsymbol{e}|^2 \quad \text{minimum}. \tag{5b}$$

In order to solve the problem of cavitating flow, the shape of the cavity must be calculated by successive iterations. The velocity field calculated by the above iteration is used so that the line on which the pressure is given becomes a streamline. Such a line (if it exists) is the trace of the points such that

$$\mathrm{d}\boldsymbol{P} \times \boldsymbol{V} = 0. \tag{6}$$

By reference to figure 2, the unknown normal distance h is defined by

$$\boldsymbol{P} = \boldsymbol{M} + h(s)\,\boldsymbol{n}(s). \tag{7}$$

By substituting (7) in (6), the value of h is defined by a linear differential equation of the first order:

$$\boldsymbol{V}\cdot\boldsymbol{t}\,\frac{\mathrm{d}h}{\mathrm{d}s} - \frac{h}{R}\,\boldsymbol{V}\cdot\boldsymbol{n} = \boldsymbol{V}\cdot\boldsymbol{n}, \tag{8}$$

where $\boldsymbol{V}$ is the velocity of the point M, and R is the radius of curvature at point M. This equation is solved numerically by first-order discretization, thus enabling the recurrence to be established for defining the new points of the boundary.

A cavity is defined by two parameters: its length l and its pressure p_c. Within the context of the hypotheses considered, there are at least three ways of expressing the closure condition:

$$\int_{(S)} \sigma\,\mathrm{d}s = 0, \quad \int_{(S')} \boldsymbol{V}\cdot\boldsymbol{n}\,\mathrm{d}s = 0, \quad h(s_E) = 0, \tag{9a–c}$$

where S' is the unknown part of the boundary (DE), (see figure 3), h is the normal position of the cavity, defined by (8) and s_E represents the curvilinear abscissa of the end of the zone of unknown geometry.

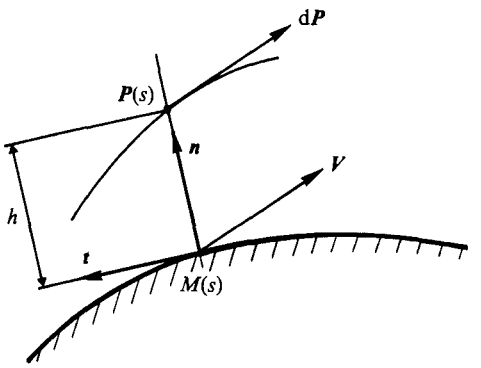

FIGURE 2. Unknown-geometry relaxation procedure (equation (8)).

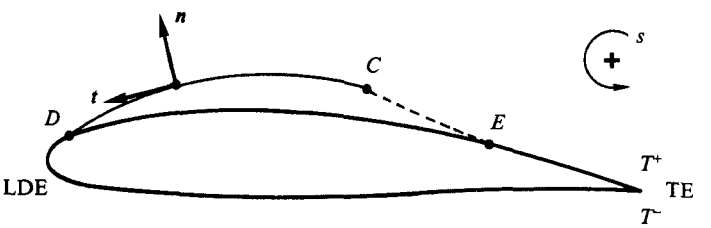

FIGURE 3. Flow model: D to C, cavity; C to E, near wake.

Equation (9a) indicates that the flow rate through the boundary is zero, while (9b) expresses the same condition written for that part of the boundary with unknown geometry, allowing the independent closure of several cavities (the condition (9a) being general). Equation (9c) is a geometrical alternative and expresses the reattachment of the streamline on the foil to the rear of zone IV. This last condition improves the convergence of the rear-cavity calculations in axisymmetrical geometry.

For the solution to the analytical problem, conditions (9a–c) are strictly equivalent to a closure condition applied to the cavity plus wake boundary. Owing to the relaxation procedure applied to this boundary and to the associated discretization errors, this equivalence is not respected for the numerical solution, especially in cases where conditions are nonlinear.

3. Partial cavitation around a thin foil

3.1. *Formulation*

Since the shape of the cavity is not known, the calculation is initiated from a geometry corresponding to the foil section. On the non-wetted side of the foil, the surface impermeability conditions are expressed by the following classic formula:

$$\boldsymbol{V}\cdot\boldsymbol{n} = 0 \quad \text{on } ET^+ \quad \text{and} \quad DT^-. \tag{10}$$

In each iteration of the cavity calculation, the tangential component of the velocity is assumed to be constant. Since the associated parameter is the cavity pressure, Bernoulli's equation is used to calculate the cavitation number:

$$K = \frac{p_\infty - p_c}{\frac{1}{2}\rho V_\infty^2}$$

using the expression

$$K = \frac{(V_{t0})^2}{V_\infty} - 1, \tag{11}$$

where V_{t0} is an unknown constant given by

$$\boldsymbol{V}\cdot\boldsymbol{t} = V_{t0} \quad \text{on } DC \tag{12}$$

In these expressions, p_∞ is the reference pressure, p_c the cavity pressure, and ρ the fluid density.

On the cavity, the velocity component normal to the cavity surface will be zero only at the convergence of the iterative process. The connecting condition related to the cavity–foil transition zone is expressed by (figure 3)

$$\left.\begin{aligned} &\boldsymbol{V}\cdot\boldsymbol{n} = \boldsymbol{V}\cdot\boldsymbol{n}\,(C) f(s), \\ &f(s_C) = 1, \\ &f(s_E) = 0. \end{aligned}\right\} \quad \text{on } CE. \tag{13}$$

The length of this zone (λ) and the function $f(s)$ are chosen arbitrarily as input data. In the absence of any accurate data concerning the wake structure, the choice of the function $f(s)$ can be restricted to the expression

$$f(s) = \left(\frac{s - s_E}{s_C - s_E}\right)^\nu; \quad \lambda = s_C - s_E, \tag{14}$$

where ν is a real positive constant. At convergence, $\boldsymbol{V}\cdot\boldsymbol{n} = 0$ on the wake boundary. It should be noted that the variation in pressure in this zone can also be imposed directly by

$$\boldsymbol{V}\cdot\boldsymbol{t} = V_{t0} f(s) + \boldsymbol{V}\cdot\boldsymbol{t}(C)\,(1 - f(s)) \quad \text{on } CE. \tag{15}$$

To these boundary conditions should be added the Joukowski condition which may be written as follows:

$$\boldsymbol{V}\cdot\boldsymbol{t}(T^+) + \boldsymbol{V}\cdot\boldsymbol{t}(T^-) = 0 \tag{16}$$

and one of the forms of the cavity closure condition (cf. (9)).

If the foil is discretized into n panels, there are $n+2$ linear conditions of type (5a), and $2n+1$ unknowns: the $2n$ singularities and the cavitation number K.

The problem (5) can be closed by the choice of vector $\mathbf{e}$ derived directly from the condition (4):

$$\boldsymbol{e} = (\sigma_1 - \sigma_n,\ \sigma_2 - \sigma_1, \ldots, \sigma_{n-1} - \sigma_n,\ \omega_1 + \omega_n,\ \omega_2 - \omega_1, \ldots, \omega_{n-1} - \omega_n). \tag{17}$$

The component $(\sigma_1 - \sigma_n)$ tends to impose a symmetrical behaviour of the sources on the foil, thereby guaranteeing satisfactory lower side/upper side decoupling.

In order to prevent non-return of the fluid at the trailing edge, the component $(\omega_1 + \omega_n)$ must be minimized. This condition is practically ensured by (16). In general, minimization of the vector (17) is sufficient for implicitly ensuring the tangential outlet condition but, when necessary, an explicit tangential outlet condition can be added.

In order to solve problem (5), $n+2$ unknowns are chosen, called 'main unknowns', that are grouped together in a single vector $\boldsymbol{x}_1$. A possible choice is

$$\boldsymbol{x}_1 = (\sigma_1,\ \sigma_2,\ \ldots, \sigma_n,\ V_{t0},\ \omega_1). \tag{18}$$

Input data		Calculated data	
Cavity	Near wake	Cavity	General
Detachment point Length l	Length λ ν exponent of λ law (cf. (14))	Geometry Cavitation number K	Velocity field C_p, C_L

TABLE 1. Description of input parameters and calculated parameters

The remaining unknowns (secondary unknowns) are grouped together in another vector, $\boldsymbol{x}_2$:

$$\boldsymbol{x}_2 = (\omega_2, \omega_3, \ldots, \omega_n). \tag{19}$$

As introduced by Hunt & Semple (1980) problem (5) can then be written as follows:

$$\left.\begin{aligned} &\boldsymbol{A}\boldsymbol{x}_1 + \boldsymbol{B}\boldsymbol{x}_2 = \boldsymbol{l}, \\ &\boldsymbol{e} = \boldsymbol{F}\boldsymbol{x}_1 + \boldsymbol{G}\boldsymbol{x}_2; \quad |\boldsymbol{e}|^2 \quad \text{minimum}. \end{aligned}\right\} \tag{20}$$

The solution is given by elimination and leads to

$$\left.\begin{aligned} &(\boldsymbol{A} + \boldsymbol{C}\boldsymbol{Q}^{-1}\boldsymbol{P})\,\boldsymbol{x}_1 = \boldsymbol{L}, \\ &\boldsymbol{x}_2 = \boldsymbol{Q}^{-1}\boldsymbol{P}\boldsymbol{x}_1, \\ &\boldsymbol{P} = (\boldsymbol{A}^{-1}\boldsymbol{C})\tilde{\boldsymbol{F}}\boldsymbol{F} - \boldsymbol{G}\boldsymbol{F}; \quad \boldsymbol{Q} = \tilde{\boldsymbol{G}}\boldsymbol{G} - (\tilde{\boldsymbol{A}}^{-1}\boldsymbol{C})\tilde{\boldsymbol{F}}\boldsymbol{G}, \end{aligned}\right\} \tag{21}$$

where a tilde denotes transposition.

By substituting values of the unknowns in (1) and relaxing the free boundary as previously described, the velocity can be calculated. Three iterations are required in order to solve the problem with reasonable accuracy. In the calculations presented here, the limit of five iterations was never exceeded.

Table 1 summarizes the input parameters of the problem and gives the parameters accessible by the model. The effect of the various parameters on the results will be discussed below.

3.2. *Results*

The model was first tested from the theoretical standpoint with a NACA 16206 foil geometry set at a 3° angle of attack in an infinite flow section. The position of the point representing the rear end of the cavity was fixed systematically at half the chord and, for the first calculations presented hereinafter, the near-wake length λ was fixed at 0.3. Figure 4(*a*) illustrates the shape of the cavity obtained for a detachment point located at the limit of appearance of low-pressure zone upstream of the cavity. When positioned any further downstream, this low-pressure zone is established. The pressure distribution associated with this cavity is shown on the inset in figure 4(*a*). Figure 4(*b*) shows the singularity distributions obtained in these conditions. It is worth noting that vorticity and sources vary rapidly near the leading edge. On the cavity, however, vorticity varies slowly because a constant-tangential-velocity condition is imposed on this line. As the sources do not introduce any discontinuity in tangential velocity – this discontinuity being produced by vorticity alone – it is found that the minimization condition correctly fulfils its role by creating or absorbing vorticity in places where this is physically necessary, i.e. in the high-curvature zone of the leading edge and in the near wake of the cavity. The conditions around the trailing edge were also checked to ensure that the sources had

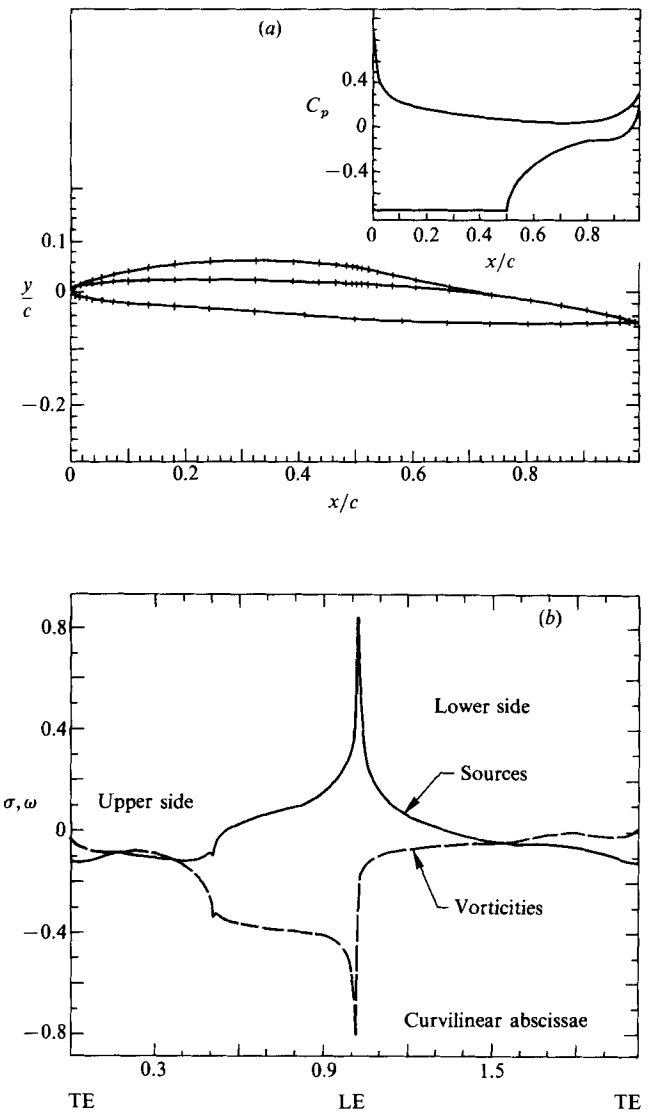

FIGURE 4. Pressure and singularities distribution for a NACA 16206: $\alpha = 3°$; $l = 0.5$; $\lambda = 0.3$. (*a*) Geometry and pressure distribution; (*b*) singularity distribution.

a symmetrical behaviour and the vorticities an antisymmetrical behaviour, guaranteeing establishment of the Joukowski condition. Finally, in the transition zones, especially at the rear of the cavity, the appearance of small oscillations was noted although these do not affect the lower side.

The geometry represented on figure 4 is probably not very realistic because of the choice of detachment-point position, located too far upstream, resulting in excessive swelling of the cavity. So the influence of the detachment-point position on cavity geometry and pressure distribution was studied, the other parameters remaining unchanged. Figure 5 shows the shape of the cavity for two detachment-point positions located respectively at $x = 0.03$ and 0.10. It can be seen that the cavity becomes flatter and that the cavity pressure increases when the detachment point is moved towards the rear of the foil. This behaviour is accompanied by the appearance

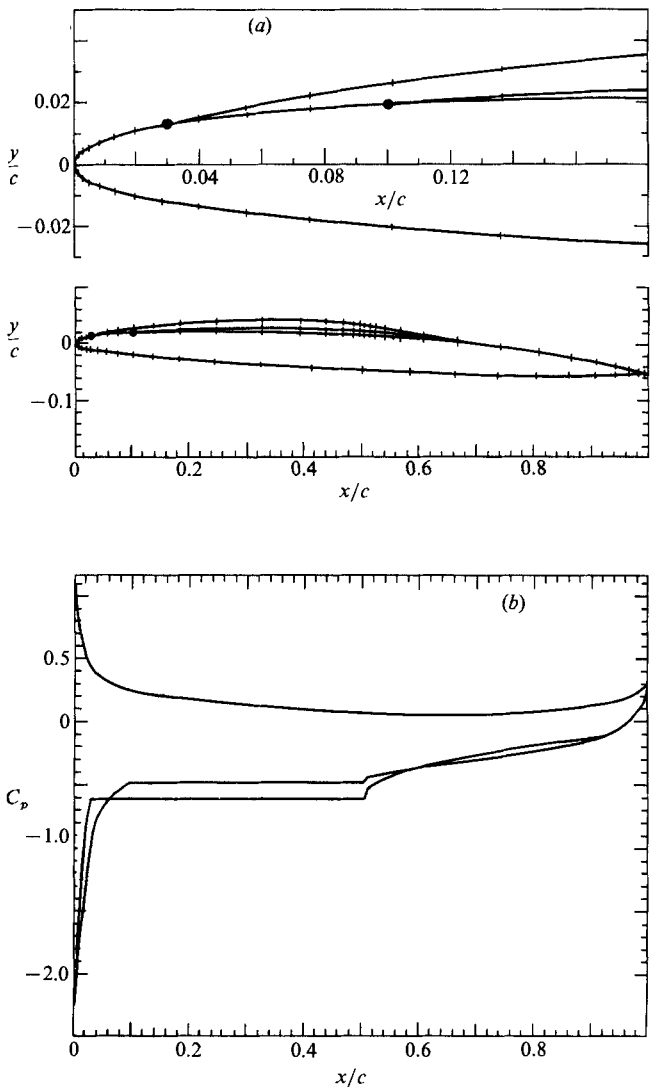

FIGURE 5. Influence of the choice of cavity detachment point on geometry and pressure distribution; $x_{\text{detach}} = 0.03$ and 0.1. (*a*) Geometry; (*b*) pressure distribution.

of a very large high-speed zone upstream of the cavity (cf. figure 5*b*) whereas the tangential outlet condition is no longer totally satisfied. The existence of an 'underpressure zone' in front of the cavity naturally leads to lifting of the first panel surface which, in certain cases, is accompanied by the appearance of a point of inflexion. This is clearly illustrated on figure 6. In this case, a cavity was calculated for a detachment point located at $x = 0.03$ assuming the foil to have an angle of attack of 6°. Here, the outlet angle is not zero but equal to 2°50′. Immediately after the first cavity panel, the existence of a point of inflexion is noted. The previous results are consistent with the theory, even if, from the physical standpoint, the cavities represented on figures 5 and 6 are probably unstable: the boundary layer will certainly not be able to withstand the high compression condition created between the maximum high-speed zone and the cavity. The pressure distribution and shape

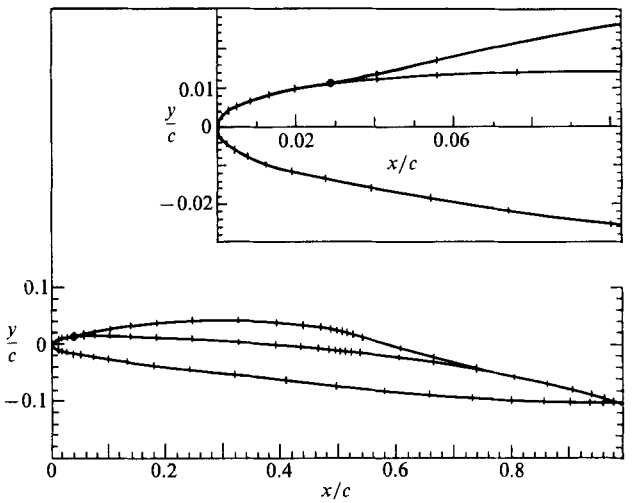

FIGURE 6. Geometry $\alpha = 6°$; $x_{\text{detach}} = 0.03$.

of associated cavities were then examined in greater detail for detachment points located near the leading edge.

Figure 7(*a*) shows the shape of the cavities obtained in this zone. The choice of a detachment point slightly downstream of point No. 28 gives rise to slight overspeed in front of the cavity. On condition that it remains restricted, as shown on figure 7(*b*), this overspeed could be representative of real conditions, as the fluid is capable of withstanding tensions over short distances. However, the recompression of the boundary layer causes laminar separation and it is precisely the existence of this separation that can be used as a criterion for finding the cavity equilibrium position (see Franc & Michel 1985). The choice of a detachment point upstream of point No. 29 leads to the appearance of a high pressure gradient in the immediate vicinity of the leading edge. At the same time, the cavity enters the foil, which is obviously unrealistic behaviour.

The slight flexibility of the model in the vicinity of the detachment point is perhaps a drawback to finding the position of this point by coupling with a local boundary-layer calculation. If this were to be so, an explicit tangential outlet condition could be added without difficulty. On the other hand, in its imposed implicit form, the tangential outlet condition can be used as a criterion for finding the position of the detachment point. In what follows, unless stated to the contrary, it is this simplified criterion that has been used.

Table 2 indicates the effect of the choice of cavity detachment point on the lift coefficient and cavitation number (see figures 7*a* and 7*b*):

$$C_p = \frac{p - p_\infty}{\frac{1}{2}\rho V_\infty^2} \tag{22}$$

$$C_L = \frac{V_\infty}{V_\infty} \cdot \int_{(s)} C_p \boldsymbol{t}\, \mathrm{d}s. \tag{23}$$

Figure 8 shows, for the same foil and same operating conditions, the effect of wake length on the pressure distribution downstream of the cavity. Here, the wake has been described by a quadratic connecting law of the normal velocity (see (13) and (14), $\nu = 2$). The length of the wake has a direct bearing on pressure recovery. For

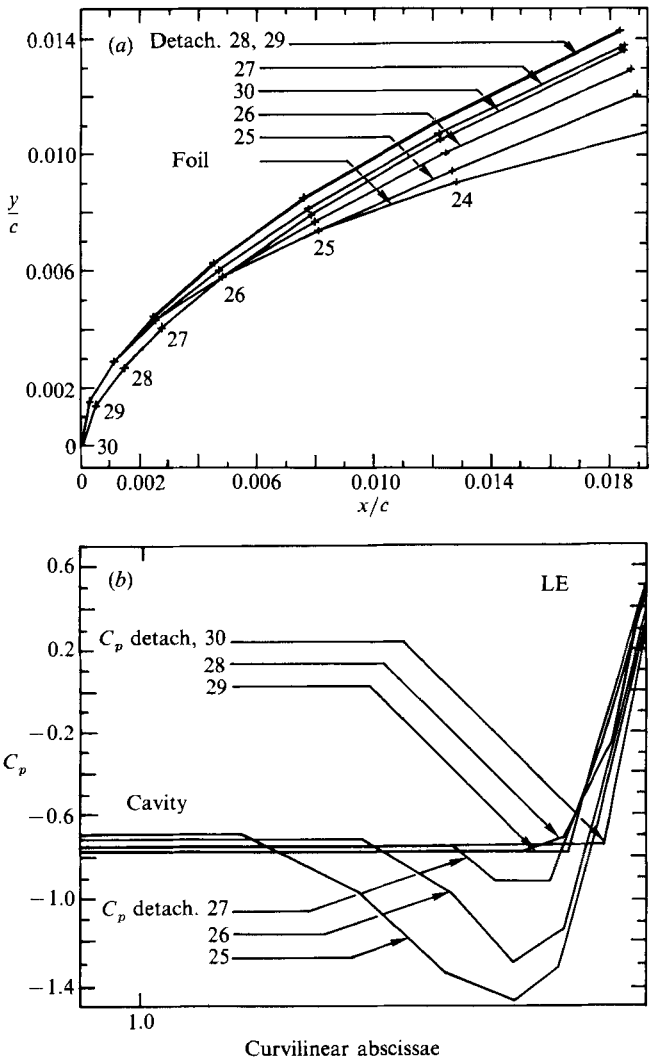

FIGURE 7. Influence of the choice of cavity detachment point on geometry and pressure distribution near the leading edge. (*a*) Shape of the cavities; (*b*) pressure distribution.

Detachment point	C_L	C_p cavity $= -K$
25	0.571	−0.711
26	0.576	−0.733
27	0.580	−0.750
28	0.583	−0.761
29	0.586	−0.766
30	0.584	−0.760

TABLE 2. Sensitivity of lift coefficient and non-dimensional pressure in the cavity to the choice of detachment point

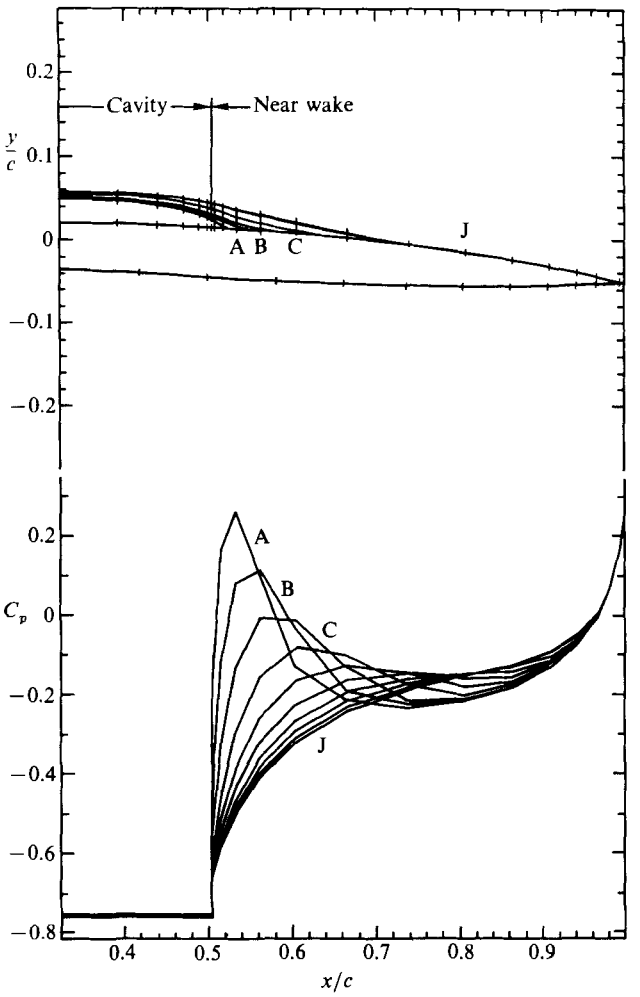

FIGURE 8. Influence of the near-wake length on geometry and pressure distribution on the rear part of the foil.

short wakes, pressure recovery is high while for long wakes, recovery can disappear. Table 3 shows the effect of wake length on the lift coefficient and cavity pressure.

The effect of the exponent ν of the connecting law (see (14)) is similar to that of the wake length. For $\nu > 2$, pressure recovery is high, which corresponds to a shortening of wake length. In what follows, a ν-value of 2 has been chosen systematically and the wake length λ was again fixed at 0.3.

The results of the present method were compared with the analytical experiments and calculations presented by Uhlman & Jiang (1977) of MIT. The foil tested has a plane lower side, a circular upper side and a 6% relative thickness. To eliminate the geometrical singularity of the leading edge, this edge was rounded with a radius of curvature relative to the chord of $r/c = 0.001$. Figures 9 and 10 show the excellent agreement between the results concerning the cavity lengths and the cavitation numbers. It is worth noting that the evolution of the $l(K)$ law in our model is identical to that of the analytical theories presented in comparison. This will be discussed later.

λ, near-wake length relative to the chord	C_L	C_p cavity $= -K$
0.07	0.563	−0.752
0.10	0.572	−0.762
0.16	0.578	−0.763
0.23	0.583	−0.761
0.30	0.590	−0.759
0.36	0.595	−0.757
0.40	0.600	−0.756

TABLE 3. Sensitivity of lift coefficient and non-dimensional pressure in the cavity to wake length

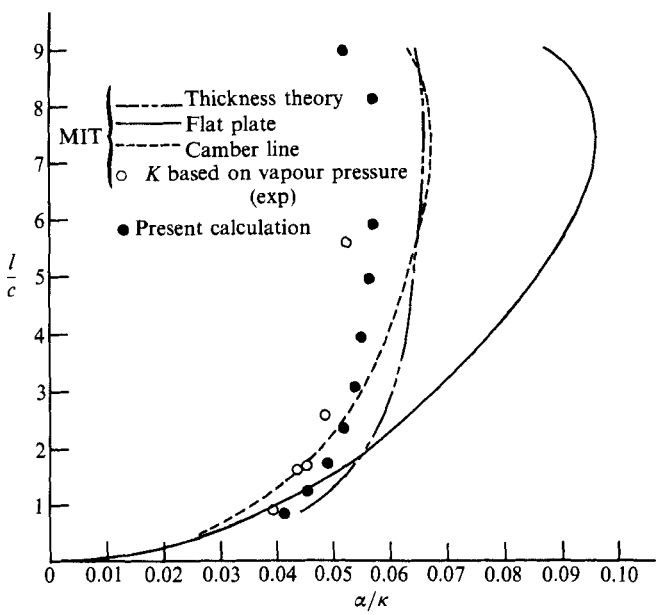

FIGURE 9. Plano-convex section, comparison with MIT results (Uhlman & Jiang 1977): cavity length *vs.* α/K for $t/c = 0.06$, $\alpha = 2°$.

A second comparison of our model was made with the experimental data obtained with a NACA 16012 by Franc. Despite the fact that our calculations do not make allowance for wall effects, there is good agreement between the NACA results and our model for short cavities ($l/c < 0.4$) (see figure 11).

The difference between the calculated pressure and the measured pressure noted for long cavities invites the following comments. Figures 9 and 10 show that, over a wide range of variation, there are two possible cavity lengths for a given pressure value. To make the flow reattach to the back of the foil is globally equivalent to an overestimation of the flow circulation around the foil and thus to a corresponding overestimation of the velocity at the cavity boundary and of the cavitation number. The analytical results given in the comparisons with MIT tests assume flow reattachment and show the same behaviour as our model. This confirms that, for large cavity lengths, the hypothesis of flow reattachment on the foil downstream of the cavity is not realistic.

For the long cavities, a cavity model was then developed in which the near wake

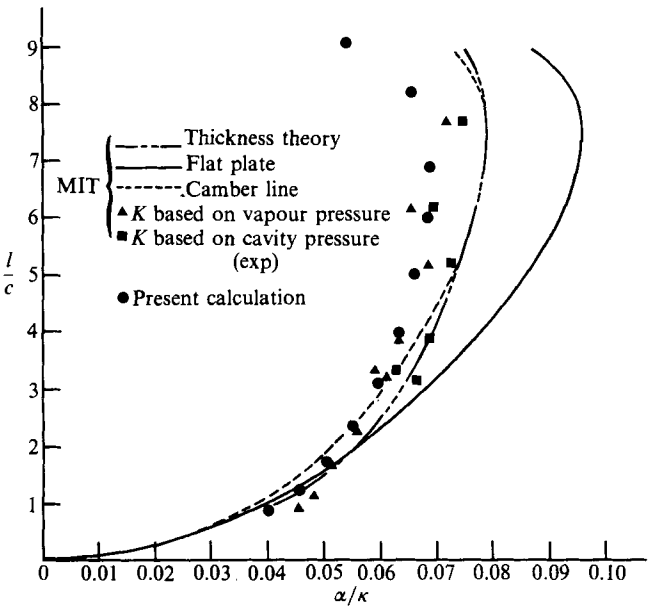

FIGURE 10. Plano-convex section, comparison with MIT results (Uhlman & Jiang 1977): cavity length *vs.* α/K for $t/c = 0.06$, $\alpha = 4°$.

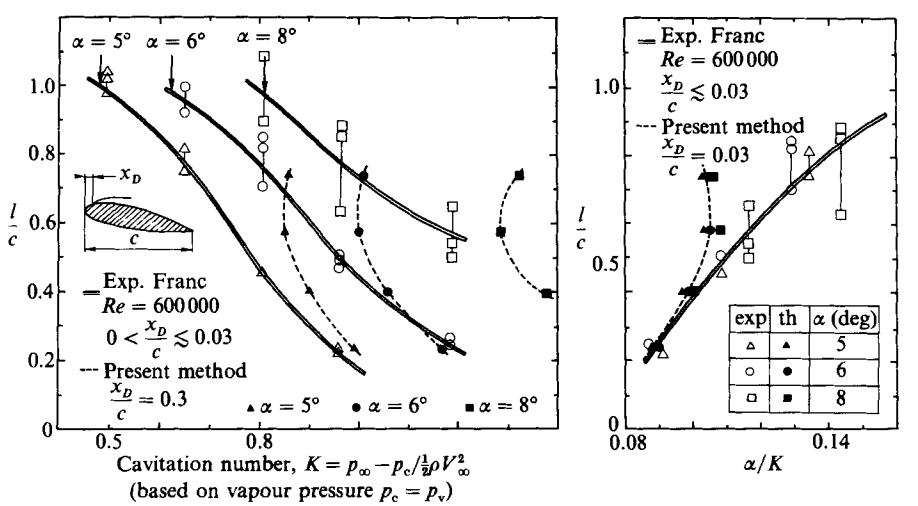

FIGURE 11. Comparison with NACA 16012.

extends downstream of the trailing edge. The results of this model are given here purely for explanatory purposes as the wake modelling method used is in fact too simplified to allow valid quantitative analysis. For cavity lengths greater than the chord, a supercavitation model similar to that presented in §4.2 was used. The results are given in figure 12. Worthy of note is the analogy in behaviour between these three models and the tests. Using the models described here, the variations in pressure can be obtained qualitatively and satisfactorily by comparison with experimental results.

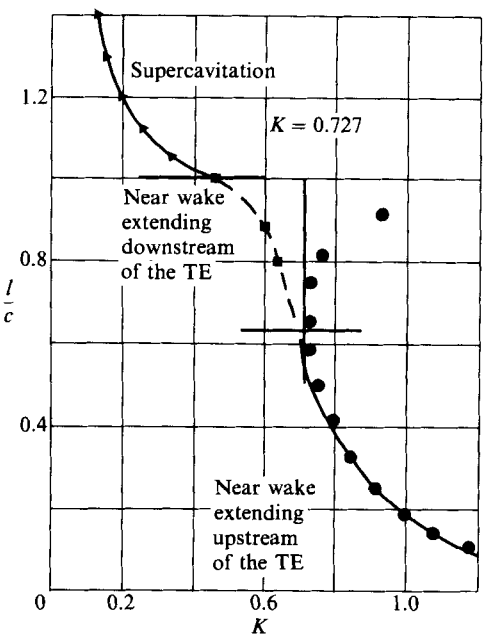

FIGURE 12. Variation of cavitation number K with cavity length.

4. Model extensions

4.1. *Cavitation behind a rounded body*

In this particular case, the calculation concerns flow around foil sections with a rounded trailing edge as might exist for hydraulic machines. Prediction of the lift of such bodies is greatly influenced by the manner in which the Joukowski condition is dealt with and the strictly potential calculation leads to an unrealistic description of the flow in the vicinity of the trailing edge. In order to take into account the existence of a wake behind the body, the recirculation zone behind the section is modelled as a cavity. This is acceptable insofar as a wake can be considered, approximately, to be a constant-pressure zone.

In order to demonstrate the flexibility of the method described in §3, and notably the fact that the number of boundary conditions is not limited to the number of panels, the wake is modelled in the form of two cavity boundaries followed by a stagnation point.

The section used for this study is a tip section of a Kaplan turbine of 3 % maximum thickness, ending in a small circle at the trailing edge, the circle diameter being equal to 5×10^{-3} chord. On such a body, the position of the cavity detachment point is determined without ambiguity on the lower side by the change in slope. It is assumed here that the separation point on the upper side is also located at the point where the curvature becomes discontinuous and the displacement thicknesses are ignored on the upper and lower sides of the foil. The initial shape of the cavity is made up of a first panel extending beyond the body, and then a straight line parallel to the velocity to infinity.

The boundary conditions are as follows: for the wetted part, the impermeability condition, (10); for the cavity, the constant-pressure condition, (11). Given the initial shape of the cavity, a tangential output condition of the cavity has been added on the first cavity panel. This is achieved by simultaneously imposing the two

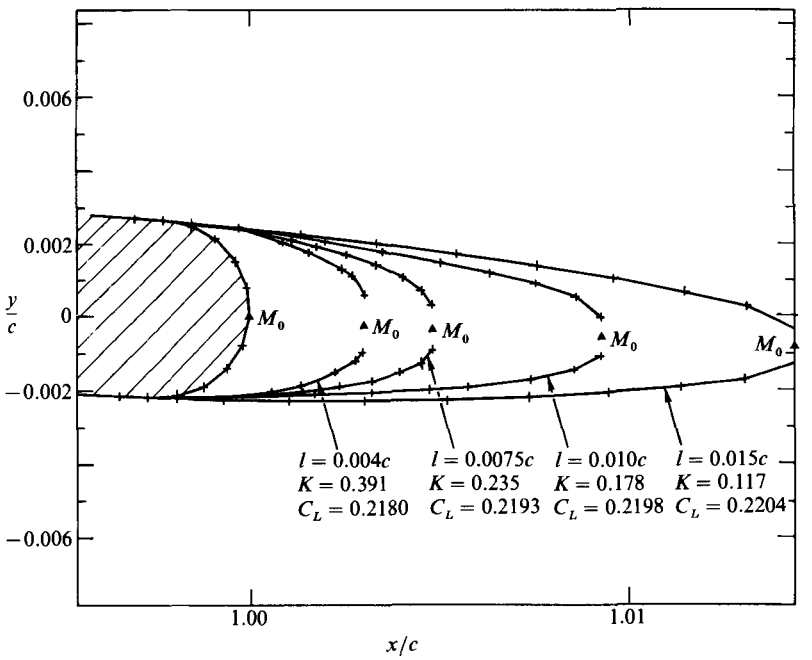

FIGURE 13. Trailing-edge cavity. Influence of the pressure on C_L.

conditions (10) and (11) on this panel. Equation (9*a*) has been used to close the cavity. Finally, the stagnation point (M_0) is described by the following conditions:

$$\left.\begin{aligned} &\boldsymbol{V}_\infty \cdot \boldsymbol{V}(M_0) = 0, \\ &\boldsymbol{V}_\infty \times \boldsymbol{V}(M_0) \cdot \boldsymbol{k} = 0 \quad (\boldsymbol{k} \text{ perpendicular to the flow plane}). \end{aligned}\right\} \tag{24}$$

The stagnation point is defined as the middle point between the ends of the cavity. For convergence requirements, the free boundary relaxation was under-relaxed, and (7) is replaced by

$$\boldsymbol{P} = \boldsymbol{M} + \Omega\, h(s)\, \boldsymbol{n}(s), \tag{25}$$

where Ω is an under-relaxation coefficient between 0.5 and 0.8 in the cases treated. The need for under-relaxation is related essentially to the instability derived from the contradiction between the fact that a value of $V = 0$ is imposed at the point M_0, whereas V = constant ($\neq 0$) on the cavity.

The problem (5) associated with the flow resolution contains $2n+1$ unknowns (as in §3) and there are $n+5$ linear constraints. It is resolved by choosing the error vector deduced from (17) by eliminating the components $(\sigma_1 - \sigma_n)$ and $(\omega_1 + \omega_n)$ since, in such case, the implicit Joukowski condition is irrelevant.

Figure 13 illustrates the rear of the section studied with a set of several cavities of different lengths. For the cavity lengths explored, the cavitation number decreases rapidly whereas the lift coefficient is not affected to any great extent (less than $\pm 0.5\,\%$ by cavity length). Consequently, it is justifiable to consider that the average value of lift, 0.219 in this case, is a reasonable estimate of the correct value which is practically independent of the wake length chosen as input data, for the position of the detachment point considered on the upper side. This result justifies the simple method often used which consists in opening the foil section to the rear by eliminating the rounded part, and leaving the sources to discharge into the flow: the

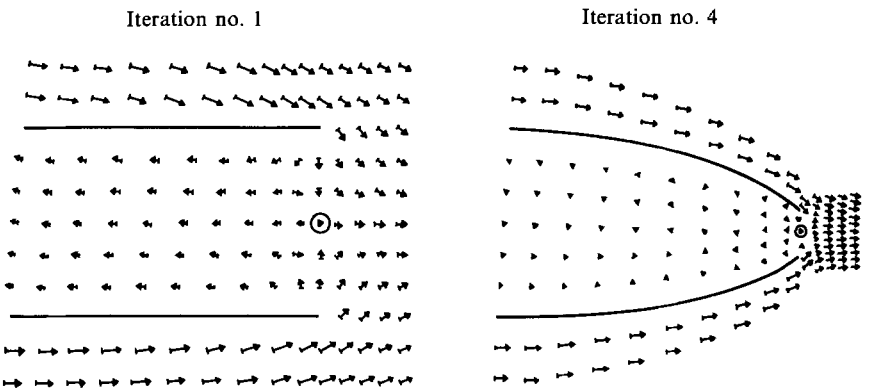

FIGURE 14. Change in velocity field near the cavity, ⊙ stagnation point. Four successive iterations.

result does not depend on the length of the wake. There nevertheless remains the problem of determining the exact position of the detachment point on the upper side.

Figure 14 shows the change in velocity field during the cavity relaxation procedure, in the vicinity of a cavity formed behind a parabolic section of 10% relative thickness. It is worth noting the influence of the stagnation point which imposes a zero velocity inside the domain assumed to represent either a wake or a cavity. Such behaviour is unrealistic, but it is clear that the model does not pretend to describe what happens at the rear of the cavity.

By combining a rear-cavitation model with the partial-cavitation model described in §3, it is possible to take into account two cavities simultaneously. This type of flow is illustrated here with respect to the geometry of axisymmetrical bodies. In such a case, given the axial symmetry, it is possible to ignore the assumed existence of a stagnation point behind the rear cavity. A partial cavitation-type closure condition is more convenient.

4.2. *Axisymmetrical body with gravity effect (one or two cavities)*

Cavitating flow around an axisymmetrical body is generally a three-dimensional problem. To extend our model to this problem without excessive modifications, the case is limited to zero angles of attack, and it is assumed that the symmetry axis of the body is identical to the direction of the gravity effect. Under these conditions, resolution of the problem is reduced to a calculation with two spatial variables on a meridian of the body and cavity, which must be a meridian of revolution. The flow speed is expressed in terms of the singularities by the following equation:

$$\boldsymbol{V}(P) = \boldsymbol{V}_\infty + \int_{(S)} \frac{\sigma(M)\,\boldsymbol{r}(M,P)}{r^3(M,P)}\,\mathrm{d}S(M) + \int_{(S)} \frac{\omega(M)\,\boldsymbol{k}\times\boldsymbol{r}(M,P)}{r^3(M,P)}\,\mathrm{d}S(M), \qquad (26)$$

where σ and ω are the surface densities of sources and vorticities, $\mathrm{d}S$ the surface element on the body, $\boldsymbol{k}$ the unit vector in the azimuthal direction with P, M and $\boldsymbol{r}$ having the same meanings as in (1).

Equation (26) is discretized in the same manner as a two-dimensional equation: the surface meridian is divided into discrete straight segments and the singularity distributions are assumed to be constant on the truncated cones defined by the surface. Two integrations are required in order to calculate the influence coefficients.

The first integration is possible analytically, giving rise to complete elliptical integrals, while the second is numerical, based on an analytical treatment according to the classic method used previously by Hess & Smith (1967).

In order to take into account the presence of two cavities at the same time, the wake model used for partial cavitation will be extended to the base cavity. In addition, the (9*c*) form of the cavity closure equation must be used.

When allowance is made for the gravity effect, the simplicity of the constant-pressure condition (11) disappears. Considers the application of the Bernoulli relation between the cavity detachment point (D) and a standard point:

$$P_M + \rho\tfrac{1}{2}(V_M)^2 - \rho g x = P_D + \rho\tfrac{1}{2}(V_D)^2 - \rho g L, \tag{27}$$

where x is the abscissa relative to the front of the body and L the body length.

The constant pressure condition on the cavity then becomes nonlinear in relation to the tangent velocity at the detachment point and is expressed as follows:

$$\boldsymbol{V}\cdot\boldsymbol{t} = V_D\left[1+\frac{2}{F}\frac{x-L}{L}\frac{(V_\infty)^2}{(V_D)^2}\right]^{\frac{1}{2}}, \tag{28}$$

$$F^2 = V_\infty^2/2gL,$$

where V_D is the velocity at the detachment point and F the Froude number based on the length L of the body.

In form, (28) is not very different from (11). Since problem resolution is iterative, the corrective term of (28) can be evaluated on the first iteration by assuming V_D is equal to V_∞. On subsequent iterations, the corrective term is evaluated with the tangential velocity calculated from the previous iteration. In this way, the condition (28) becomes linear with respect to the velocity at the detachment point V_D:

$$\boldsymbol{V}\cdot\boldsymbol{t} = V_D\, k(x), \tag{29}$$

where $k(x)$ is a known function of the abscissa, of order one.

On presenting the wake-cavity model in §4.1, the usefulness of under-relaxing the calculation of the position of the boundary was indicated. In the present case, the boundary conditions (28) and the geometry must be adjusted simultaneously. Consequently, to be sure of satisfactory convergence of the iterative process, the convergence speed should be controlled by a less coarse means. The closure condition is adjusted progressively.

Equation (9*c*), or more exactly its adaptation to the base-cavity problem, can be used for fine adjustment of convergence speed. This equation is strictly expressed for the base cavity as follows:

$$h(E) = -y(E), \tag{30}$$

where h has the same meaning as in (8) and y is the rear ordinate.

The closure condition effectively applied is expressed by

$$h(E) = -\Omega\, y(E), \tag{31}$$

where Ω is a coefficient between 0 and 1. The need to adjust the closure condition progressively is related to the fact that the problem depends on two unknowns: one concerning the geometry and the other concerning the function to be distributed on this geometry. The procedure amounts to allowing the function to adjust correctly before too great a deformation of the geometry occurs.

Thus, if Ω is equal to 1, the cavity closes at the first iteration without condition

(28) being satisfied with sufficient accuracy. If Ω is equal to zero, a simple redistribution of the points of the boundary around the initial position takes place and (28) can be applied to obtain a much better estimate of the cavity pressure. In cases where the gravity effect is very high (F of the order of, or less than, one, and cavity length of the same order as that of the body), a value of $\Omega = 0$ is imposed on the first iteration, followed by a value between 0.6 and 0.8 for subsequent iterations. Despite its simplicity, (30) is nonlinear and must be slightly modified. Equation (8) is equivalent to

$$\frac{\mathrm{d}h}{\mathrm{d}s} = \frac{\boldsymbol{V}\cdot\boldsymbol{n}}{\boldsymbol{V}\cdot\boldsymbol{t}}\left(1+\frac{h}{R}\right). \tag{32}$$

The tangential velocity is evaluated according to the same rules as for (28). The cavity is initially cylindrical and, as such, the curvature of the meridian is zero. In subsequent iterations, it is reasonable to assume that the solution is close and that, as a result, the deflection h of the cavity is much smaller than the radius of curvature of the meridian. The equation for closure of the under-relaxed cavity can then be written as follows:

$$h(E) = \int_{(D)}^{(E)} \frac{\boldsymbol{V}\cdot\boldsymbol{n}}{\boldsymbol{V}\cdot\boldsymbol{t}}\,\mathrm{d}s = -\Omega y(E). \tag{33}$$

The boundary conditions are therefore summarized by the application of (11) to the wetted part of the body, (28) to the cavity and (13) to the cavity wake. This set of equations is complemented by (33). To complete definition of the problem (5), the vector chosen to be minimized is

$$\boldsymbol{e} = (\sigma_1-\sigma_2, \ldots \sigma_{n-1}, \omega_1-\omega_2, \ldots, \omega_{n-1}-\omega_n, \omega_n), \tag{34}$$

where 1 and n represent respectively the number of the last control point on the wake (point E) and the first control point of the body. This form is the natural restriction of (17) to the axisymmetrical geometries.

Again, it is interesting to note that it is not necessary to impose the tangential outlet condition on either side of the cavity detachment point. Continuity is obtained naturally by the model. Figure 15 shows a series of cavities behind an elongated section (ellipse-cylinder). The effect of gravity is shown by the existence of overpressure cavities ($K < 0$). These cavities adopt a bulging shape with diameter exceeding the middle diameter of the body.

Figure 16 illustrates a typical pressure distribution on the meridian of the body. If $V_M = V_\infty$, then C_p is reduced to its hydrostatic component, equivalent to the pressure in the absence of a body (straight line). The parts of the curve below the straight line are equivalent to overspeed conditions. Consequently, there is a risk of cavitation in these zones. The calculations needed five iterations and the pressure plateau in the cavity bears witness to the satisfactory convergence of the calculation. Figure 17 gives the variation in cavity pressure as a function of cavity length (with Froude number as a parameter, see definition in (28).

It is possible to calculate two cavities on the body simultaneously. The rear cavity may be caused by the existence of gas, of given pressure, and the front cavity may be caused by fluid acceleration (notably in the case of a break in slope). As before, the two cavity lengths are given (l_1 and l_2) as well as their wake lengths, whereby two different tangential velocities at the two detachment points are available. It is necessary to apply the condition (28) with the corresponding tangential velocities V_{D1} and V_{D2} and to have two cavity closure equations. Equation (9b) is used for the

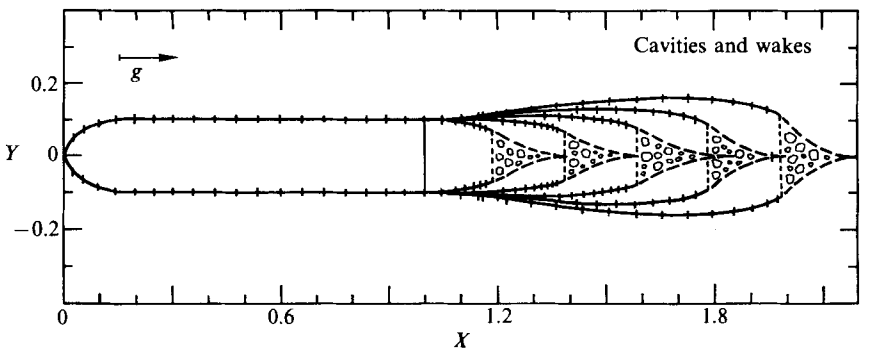

FIGURE 15. Rear cavity – axisymmetrical body ($F = 2$).

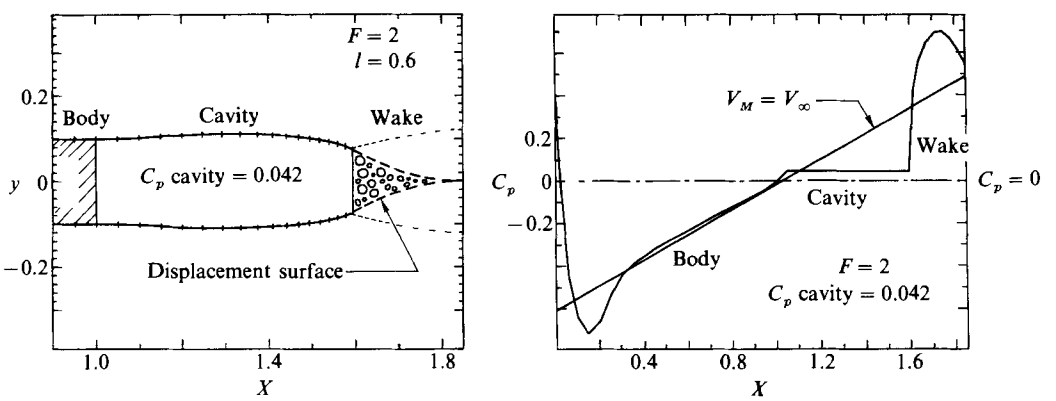

FIGURE 16. Typical pressure distribution with gravity effect.

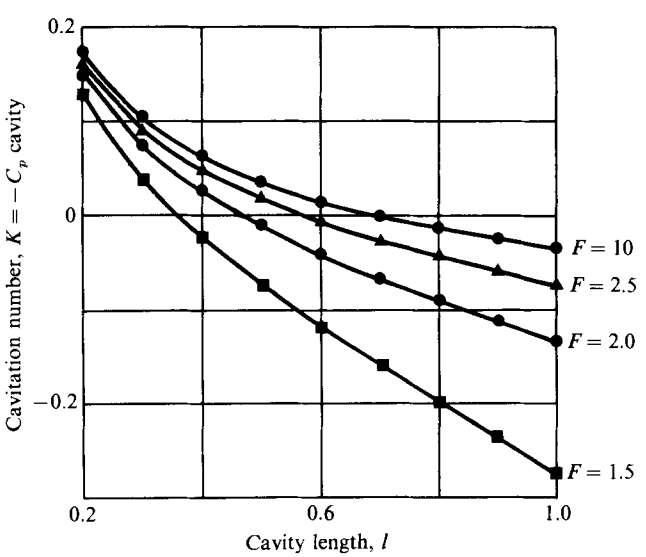

FIGURE 17. Variation in cavity pressure in relation to cavity length and Froude number.

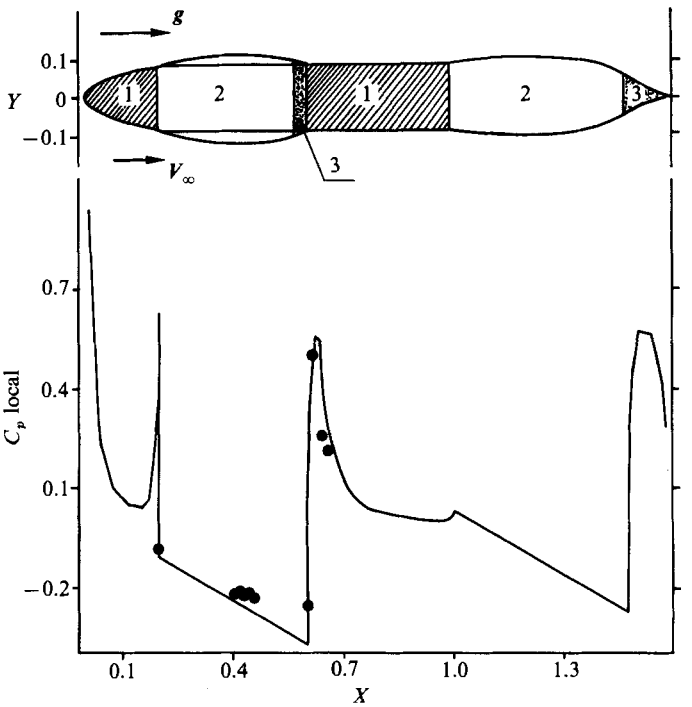

FIGURE 18. Typical pressure distribution with two cavities. Exp. ● (NEYRTEC). 1, axisymmetric body: impermeability condition; 2, cavity: constant pressure; 3, near wake: displacement thickness. C_p local $= P - P_{\text{hydrostatic}}/\frac{1}{2}\rho V_\infty^2$.

front cavity and (31) for the rear cavity. It is then relatively easy to adjust the two cavity lengths to obtain the desired pressures. Figure 18 shows a typical example of such a calculation.

5. Conclusions

The Minimization Process Panel Method (MPPM) proves to be particularly well suited to describing cavitating flows in complex situations. Realistic outlet conditions with a low discretization error can be obtained by minimizing the gradients. This is particularly interesting for thin structures. Since the number of boundary conditions to be satisfied does not depend on the number of control points, the method can be adapted to a variety of situations. This feature, coupled with the incorporation of a far wake, would give open semi-empirical models (fixed l, K law). The recompression law can be adjusted through the near wake whereas the dissipative effects could be taken into account by the far wake, not introduced in the present study. By using a geometric closure condition with an exact numerical definition for the discrete problem, several cavities can be taken into account simultaneously, even when gravity aggravates the nonlinearity of the problem. By coupling this method with a boundary-layer calculation, it would be possible to calculate the position of the cavity detachment point on the basis of the laminar-separation criterion. There are no theoretical difficulties in extending the method to three-dimensional or unsteady flow conditions. The most urgent work to be carried out involves determining how to choose the data corresponding to the near and far wakes so as to match theoretical

results with experimental results. Such work cannot be validly carried out without proven data concerning the structure of the wake behind the cavity. At the present time, more extensive data are needed in this respect.

The authors would like to thank Mr Kenn, Head of the Hydraulics Laboratory of Imperial College, London, and Dr Graham, of the Aeronautics Department, for the valuable advice and for the abundant literature that they so kindly provided. This study was financed in part by the 'Direction des Recherches, Etudes et Techniques' (Contract no. 80.414).

REFERENCES

CHANG-SUP, L. 1980 Prediction of the transient cavitation on marine propellers by numerical lifting-surface theory. In *thirteenth Symposium on Naval Hydrodynamics, Tokyo, October 1980* Vol. 1 (ed. T. Inui), pp. 41–64. Shipbuilding Research Association of Japan.

FRANC, J. P. & MICHEL, J. M. 1985 Attached cavitation and the boundary layer: experimental investigation and numerical treatment. *J. Fluid Mech.* **154**, 63–90.

FURNESS, R. A. & HUTTON, S. P. 1975 Experimental and theoretical studies of two-dimensional fixed-type cavities. *Trans. ASME* I: *J. Fluids Engng* **97**, 515–522.

FURUYA, O. 1975*a* Non-linear calculation of arbitrarily shaped supercavitating hydrofoils near a free surface. *J. Fluid. Mech.* **68**, 21–40.

FURUYA, O. 1975*b* Three-dimensional theory on supercavitating hydrofoils near a free surface. *J. Fluid Mech.* **71**, 339–359.

FURUYA, O. 1980 Non-linear theory for partially cavitating cascase flows. In *IAHR 10th Symp.*, Tokyo, pp. 221–241.

GOLDEN, D. W. 1975 A numerical method for two-dimensional cavitating lifting flow. In *M.I.T. Department of Ocean Engineering, Rep.* 81512-1.

HESS, J. L. & SMITH, A. M. O. 1967 Calculation of potential flow about arbitrary bodies. *Prog. Aero. Sci.* **8**, 1–137.

HUNT, B. & SEMPLE, W. G. 1980 The panel method for subsonic aerodynamic flows: a survey of mathematical formulations and numerical models and an outline of the new British Aerospace Scheme. In *Computational Fluid Dynamics* (ed. W. Kollmann), vol. I, pp. 99–166. Hemisphere.

LAROCK, B. E. & STREET, R. 1967 A non-linear solution for a fully cavitating hydrofoil beneath a free surface. *J. Ship Res.* **11**, 131–139.

LEEHEY, P. 1973 Supercavitating hdrofoil of finite span. *IUTAM Symp, Leningrad* (ed. L. J. Sedov & G. Y. Stepanov), pp. 277–299. Moscow: Nauka.

NISHIYAMA, T. & ITO, J. 1977 Calculation of partially cavitating hydrofoils by singularity method. Part 1. Two-dimensional isolated hydrofoils. *Trans JSME* **43**, 2165–2174.

NISHIYAMA, T. & MIYAMOTO, M. 1969 Lifting-surface method for calculating the hydrodynamic characteristics of supercavitating hydrofoil operating near the free water surface. *Tech. Rep. Tohoku University* **34**, pp. 123–139.

PELLONE, C. & ROWE, A. 1981 Supercavitating hydrofoils in non-linear theory. In *Third Intl Conf. on Numerical Ship Hydrodynamics, Paris, June 1981* (ed. J. C. Dern & H. J. Haussling). Bassin d'essais des Carènes, Paris, France.

TSEN, L. F. & GUILBAUD, M. 1974 A theoretical and experimental study on the planform of superventilated wings. *J. Ship Res.* **18**, 169–184.

TULIN, M. P. 1953 Steady two-dimensional cavity flows about slender bodies. In *David W. Taylor Mod. Basin Rep.* 834.

TULIN, M. P. 1964 Supercavitating flows, small perturbation theory. *J. Ship Res.* **7**, 16–37.

UHLMAN, J. S. & JIANG, C. W. 1977 Experiments on a partially cavitating planoconvex hydofoil with comparison to theory. *MIT, Department of Ocean Engineering, Rep.* 83481–2.

VERRON, J. 1979 Ecoulements cavitants autour d'ailes d'envergure finie en présence d'une surface libre. *J. Méc.* **18**, 745–773.

WIDNALL, S. E. 1966 Unsteady loads on supercavitating hydrofoils of finite span. *J. Ship Res.* **10,** 107–118.

WU, T. Y. T. 1956 A free streamline theory for two-dimensional fully cavitated hydrofoils. *J. Maths Phys.* **35**, 236–265.

WU, T. Y. T. 1959 A note on the linear and non-linear theories for fully cavitated hydrofoils. In *Calif. Inst. Technol., Hydrodrynamic Lab. Rep.* 21. 22.

YAMAGUCHI, H. & KATO, H. 1983 On application of non-linear cavity flow theory to thick foil sections. In *Second Conf. on Cavitation, Edinburgh* 6–8 *Sept.* 1983, pp. 167–174. Institution of Mechanical Engineers.